Optics Letters

Fiber-optic electron-spin-resonance thermometry of single laser-activated neurons

A. A. Lanin,[1,2,3] I. V. Fedotov,[1,2,3] Yu. G. Ermakova,[4] D. A. Sidorov-Biryukov,[1,3] A. B. Fedotov,[1,3] P. Hemmer,[2] V. V. Belousov,[4] and A. M. Zheltikov[1,2,3,5,*]

[1]Physics Department, International Laser Center, M.V. Lomonosov Moscow State University, Moscow 119992, Russia
[2]Department of Physics and Astronomy, Texas A&M University, College Station, Texas 77843, USA
[3]Russian Quantum Center, ul. Novaya 100, Skolkovo, Moscow Region 143025, Russia
[4]M.M. Shemyakin and Yu.A. Ovchinnikov Institute of Bioorganic Chemistry, Russian Academy of Sciences, Moscow 117997, Russia
[5]Kurchatov Institute National Research Center, Moscow 123182, Russia
*Corresponding author: zheltikov@physics.msu.ru

Received 9 August 2016; revised 1 September 2016; accepted 2 September 2016; posted 2 September 2016 (Doc. ID 273389); published 29 November 2016

Optically detected electron spin resonance in fiber-coupled nitrogen–vacancy (NV) centers of diamond is used to demonstrate a fiber-optic quantum thermometry of individual thermogenetically activated neurons. Laser-induced temperature variations read out from single neurons with the NV-diamond fiber sensor are shown to strongly correlate with the fluorescence of calcium-ion sensors, serving as online indicators of the inward Ca^{2+} current across the cell membrane of neurons expressing transient receptor potential (TRP) cation channels. Local laser heating above the TRP-channel activation threshold is shown to reproducibly evoke robust action potentials, visualized by calcium-ion-sensor-aided fluorescence imaging and detected as prominent characteristic waveforms in the time-resolved response of fluorescence Ca^{2+} sensors.

OCIS codes: (060.2300) Fiber measurements; (060.2370) Fiber optics sensors.

http://dx.doi.org/10.1364/OL.41.005563

Temperature is a fundamental objective measurable whereby the universal physical principles, including the laws of thermodynamics, enter into biology, controlling every biological process within a living organism and within each living cell [1]. In the nervous system, thermosensitive ion channels in cell membranes—transient receptor potential (TRP) cation channels [2]—serve as elementary heat-controlled actuators, which convert incoming energy into action potentials, thus enabling the sensation of warm, cold, and hot [3–6]. In a more detailed picture of temperature effects in neuronal circuits, conduction of action potentials, presynaptic transmitter release, and postsynaptic reception are all highly sensitive to temperature, varying neuronal functions dramatically in response to temperature changes [7].

To fully understand the operation of TRP channels as tools for controlled neurostimulation [8–13] and to monitor their thermodynamic state, highly accurate and extremely delicate instruments are needed for local temperature measurements. Within the past few years, several promising and elegant approaches have been demonstrated to enable single-cell and intracellular thermometry using appropriate thermosensitive fluorophores [14], fluorescent proteins [15], gold nanoclusters [16], quantum dots [17], diamond [18], silica [19], and polymer [20] nanoparticles. However, to be compatible with the research aimed at understanding the most complex functions of the higher nervous system, including learning and memory, single-neuron thermometry has to be implemented in a format that would enable efficient minimally invasive neurostimulation in freely behaving animal models. This challenge can be confronted, as shown below in this Letter, by coupling small-size temperature-sensing agents to a specifically designed fiber-optic probe and incorporating this instrument into the framework of laser-assisted thermogenetics, enabling single-cell neurostimulation with cloned and genetically encoded TRP channels.

In what follows, we demonstrate a fiber-optic quantum thermometry of individual thermogenetically activated neurons based on an optically detected magnetic resonance (ODMR) in fiber-coupled nitrogen–vacancy (NV) centers [18,21,22]. Laser-induced temperature variations read out from single neurons with the NV-diamond fiber sensor will be shown to strongly correlate with the fluorescence of calcium-ion sensors, serving as online indicators of the inward Ca^{2+} current across the cell membrane of TRP-expressing neurons.

A fiber-optic temperature sensor in our experiments integrates a 50-μm-core-diameter, NA ≈ 0.22 optical fiber, an NV-diamond microcrystal, and a two-wire microwave transmission line [11]. To measure the temperature of individual laser-activated neurons (Fig. 1), ground-state NV centers in diamond are polarized by 633-nm continuous-wave He–Ne-laser radiation transmitted through the optical fiber, while their spin sublevels are coupled by a microwave field delivered through the two-wire transmission line. The photoluminescence (PL) emitted as a result of laser-induced population transfer from

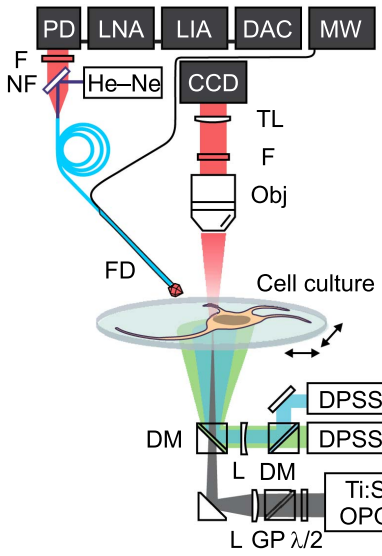

Fig. 1. Fiber-optic thermometry of single thermogenetically activated neurons: Ti:S, mode-locked Ti:sapphire laser; OPO, femtosecond optical parametric oscillator; GP, Glan prism; $\lambda/2$, half-wave plate; DM, dichroic mirror; L, lens; DPSSL, diode-pumped solid-state laser; FD, fiber probe with an NV-diamond quantum temperature sensor; Obj, microscope objective; F, filters; He–Ne, helium–neon laser; MW, microwave source; LNA, low-noise amplifier, LIA, lock-in amplifier; DAC, data acquisition circuit; T, telescope; NF, notch-filter; TL, tube lens; PD, photodetector; CCD, CCD camera.

the ^3A ground state to the ^3E excited state of NV centers features a well-resolved peak of the zero-phonon line at approximately 637 nm, detected against a broad background of the phonon-sideband line. The same optical fiber is used to collect the PL from NV centers (Fig. 1) and to transmit this signal to the detection system, consisting of a silicon photodiode, a low-noise preamplifier, a lock-in amplifier, an analog-to-digital converter, and a data acquisition card. The PL signal from NV centers in diamond is separated from the excitation laser radiation with a notch filter and a set of bandpass filters.

As the temperature of diamond increases, following the temperature in the ambient medium, the profile of the zero-external-magnetic-field ODMR is shifted toward lower microwave frequencies [Fig. 2(a)], enabling highly sensitive local temperature measurements. To provide a spatial resolution of these measurements adequate to *in situ* thermometry of individual neurons in thermogenetic studies, NV-diamond microcrystals with a diameter of 20–30 μm were used as a part of a fiber-optic thermometer used for these experiments. For the highest sensitivity and the highest speed of local temperature measurements in a cell culture, frequency-modulated microwave spin excitation in NV centers was combined with properly optimized differential lock-in detection [11,22], with an 863-Hz reference signal used to modulate the amplitude of the microwave field and demodulate the output of the lock-in amplifier.

In a calibration experiment, the fiber thermometer was placed inside a 1-l water-filled tank in such a way as to exclude any effects related to temperature gradients near the tank walls. Fiber-optic ODNR temperature measurements were then validated against the readings of a microneedle-type thermocouple, providing an accuracy of temperature measurements within 0.1°C. As can be seen from Fig. 2(b), a linear function

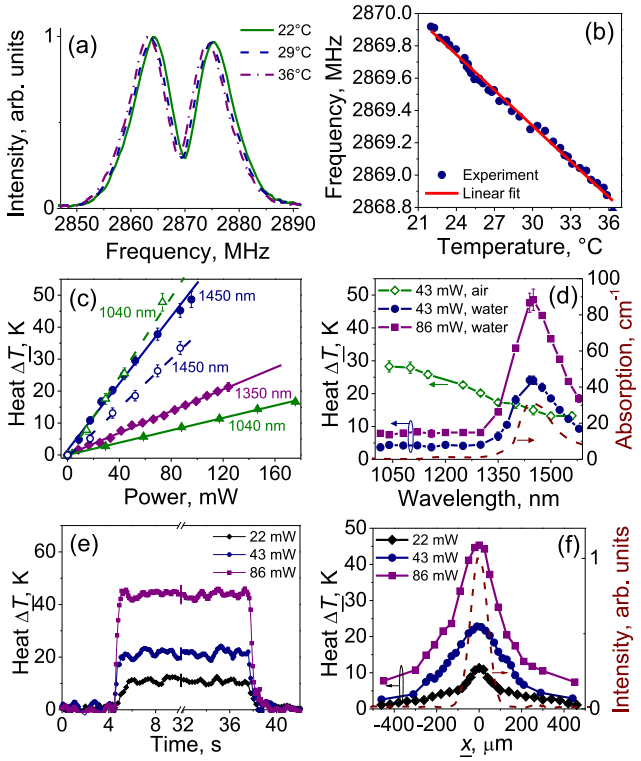

Fig. 2. (a) Intensity of PL from NV centers in a diamond microcrystal on the fiber tip measured as a function of the frequency of the microwave field at an ambient temperature of 22°C (green), 29°C (blue), and 36°C (maroon). (b) The central frequency of the ODMR spectrum of NV centers in diamond measured as a function of the ambient temperature (filled circles) and its best linear fit (solid line). (c) Laser-induced temperature change ΔT of water (filled circles, triangles, and diamonds) and the NV-diamond microcrystal in air (open circles and triangles) measured as a function of the power of heating OPO radiation with $\lambda \approx 1040$ nm (triangles), 1350 nm (diamonds), and 1450 nm (circles) with best linear fits shown by solid and dashed lines. (d) Absorption spectrum of water (dashed line) versus the temperature change ΔT induced by the OPO output in a Petri dish filled with water by 43-mW (circles) and 86-mW (rectangles) OPO radiation measured as a function of the OPO wavelength λ. The $\Delta T(\lambda)$ dependence for the NV-diamond crystal in air irradiated by a 43-mW OPO beam is shown by diamonds. (e) ΔT in an OPO-irradiated area inside a water-filled Petri dish measured as a function of time t with a mechanical shutter unblocking the laser beam at $t \approx 4.45$ s and blocking the beam at $t \approx 37.4$ s with $\lambda \approx 1450$ nm and $p = 22$ mW (diamonds), 43 mW (circles), and 86 mW (rectangles). (f) ΔT in a water-filled Petri dish as a function of the transverse coordinate x across a focused OPO beam with $\lambda \approx 1450$ nm and $p = 22$ mW (diamonds), 43 mW (circles), and 86 mW (rectangles). The dashed line is the transverse field intensity profile across the focused OPO beam.

with a slope $d\Omega_s/dT \approx -73 \pm 1$ kHz/K provides an ideal fit for this dependence within the entire temperature range of interest, viz., from 22°C to 37°C, offering a convenient calibration for temperature measurements using our fiber-optic probe with NV diamond.

Laser-induced heating was provided in our experiments by the wavelength-tunable output of a femtosecond optical parametric oscillator (OPO) pumped by sub-60-fs, 40-nJ, 808-nm, 78-MHz pulses from a mode-locked Ti:sapphire oscillator

(Fig. 1). The OPO was adjusted to deliver 100- to 150-fs pulses with a typical energy of 6 nJ at a pulse repetition rate of 78 MHz, covering the wavelength range from 1020 to 1580 nm as its signal-wave output and from 1680 to 2100 nm as its idler-wave output.

The fiber probe is placed at a distance of less than 10 μm from a targeted neuron. Once the ODMR-based temperature readings of the fiber-optic probe have reached an equilibrium level, indicating a thermal equilibrium in the cell-culture–fiber-probe system, temperature measurements are performed with a laser heating of neurons in the culture provided by the wavelength-tunable OPO source and low-power He–Ne-laser radiation used to read out the ODMR from NV centers in diamond. In Fig. 2(c), we present the difference $\Delta T = T - T_0$ between the temperatures T and T_0 measured, respectively, with and without laser irradiation of the sample as a function of the OPO output power p for different central wavelengths λ of the OPO output. For any λ, ΔT is seen to grow linearly with p, fully consistent with the standard heat-conduction model [22]. As the OPO output wavelength λ is increased from 1020 to 1580 nm, the laser-induced heating grows [cf. triangles, diamonds, and circles in Fig. 2(c)]. The $\Delta T(\lambda)$ dependences measured in the same experiment for different OPO output powers [circles and rectangles in Fig. 2(d)] closely follow the absorption spectrum of water [the dashed line in Fig. 2(d)], showing that laser-induced heating is dominated by the absorption of infrared (IR) light by water, with the heating rate per unit laser power within the studied range of laser intensities estimated as 0.52 ± 0.03 K/mW for $\lambda \approx 1450$ nm. Notably, when the NV-diamond microcrystal is heated by laser radiation in atmospheric air, the laser-induced heating ΔT monotonically decreases [open circles in Fig. 2(d)] as the laser wavelength grows from 1040 to 1450 nm [see also open circles and open triangles in Fig. 2(c)], i.e., as λ is tuned away from the resonance with the 1042-nm zero-phonon line of the singlet–singlet transition of NV centers in diamond [23].

In Fig. 2(f), we present typical steady-state profiles of ΔT measured by scanning the fiber probe along the transverse coordinate x across the area irradiated with the 1450-nm OPO output focused into an 80-μm spot. The locality of laser-induced heating is seen to be high enough to provide excitation of individual neurons in a culture with a typical distance between TRPA1-expressing neurons of about 100 μm. In Fig. 2(e), we plot the laser-induced heating ΔT measured as a function of time t with a mechanical shutter unblocking the laser beam at $t \approx 4.45$ s and blocking the beam at $t \approx 37.4$ s. The typical turn-on–turn-off time of the shutter is about 30 ms. Based on these measurements, the ΔT build-up half-time in the sample is estimated as 780 ms, 360 ms, and 170 ms for $p \approx 22$ mW, 43 mW, and 86 mW, respectively.

Experiments demonstrating *in situ* fiber-optic thermometry of individual thermogenetically activated neurons were performed on cultured mouse neurons expressing TRPA1 channels from *Crotalus atrox* western diamondback rattlesnakes, providing thermogenetic neurostimulation above the channel activation threshold $T_a \approx 28$°C [24]. The neuron cultures were prepared following the procedures and protocols described in Ref. [25]. The neurons in these cultures were co-transfected with tdTomato and GCaMP6s sensors for fluorescence visualization of TRPA1 channel expression (through a red fluorescence signal from tdTomato linked to TRPA1 via P2A autoproteolitic sequence) and the buildup of the inward Ca^{2+} current across the neuronal membrane (through green fluorescence from GGaMP6s).

In our experimental scheme (Fig. 1), the frequency-tunable output of OPO is focused with a long-focal-length lens into a beam diameter of about 80 μm. For the highest efficiency and minimum phototoxicity of laser heating, the central wavelength of the OPO output is tuned to the local maximum of water absorption at 1450 nm. The phototoxic effects and uncontrollable heat release are further reduced by using ultrashort near-IR pulses for laser irradiation. For a thermogenetic photostimulation of neurons in the culture, the OPO output is modulated with a mechanical shutter or an electro-optical chopper, yielding trains of 150-fs near-IR pulses with a tunable pulse-train duration and tunable pulse-train repetition rate.

Fluorescence imaging of thermogenetically activated neurons used a home-built upright microscope (Fig. 1), where loosely focused continuous-wave 50-mW radiation at 473 and 532 nm, delivered by diode-pumped solid-state laser sources, is used for the wide-field excitation of GCaMP6s and tdTomato fluorescent biomarkers. The fluorescence from GCaMP6s and tdTomato biomarkers is collected with a 20×, 1.05-NA objective and detected by a charge-coupled device (CCD) camera with an exposure time of 0.9 s. A GCaMP6s fluorescence image of an OPO-radiation-activated neuron overlaid with a tdTomato fluorescence image of the same neuron is presented in Fig. 3(a).

Results of laser neurostimulation experiments with *in situ* fiber-optic thermometry are presented in Figs. 3(a)–3(f). With the temperature T within the OPO-irradiated area in the culture maintained below the TRPA1 activation threshold T_a, no systematic increase in GCaMP6s fluorescence is detected, indicating no persistent neuron activation in the system. The spontaneous activity of individual neurons, on the other hand, rapidly grows as the temperature T approaches T_a [$T \approx 27.4$° in Fig. 3(b)], as indicated by random spikes of GCaMP6s fluorescence. Above the TRPA1 activation threshold, the neuronal activity pattern is drastically different. With the temperature within the laser-irradiated area in the culture increased in a stepwise fashion with a 1° increment, as shown by the dashed line in Fig. 3(c), the GCaMP6s fluorescence signal from this area is seen to steeply build up precisely when the last 1° step in Fig. 3(c) causes the temperature in the laser-irradiated area inside the culture to rise above the TRPA1 activation threshold. This increase in GCaMP6s fluorescence indicates an intense Ca^{2+} influx into neurons through the neuronal membrane [Fig. 3(c)]. With the temperature within the laser-irradiated area kept equal to T_a, the GCaMP6s fluorescence signal is seen to gradually decay [Figs. 3(c) and 3(e)], which is most likely related to a dissociation of Ca^{2+} in GCaMP6s. Measurements with control neurons, designed to express only the GCaMP6s biomarker, but no TRPA1 channels, show no increase in GCaMP6s fluorescence [Fig. 3(d)] even for temperatures T well above T_a, indicating no neuron activation.

Pulsed irradiation of samples was performed in our experiments by using a chopped OPO output, delivering sequences of millisecond trains of 78-MHz, 150-fs pulses of the 1450-nm OPO output with a tunable duration τ_t and tunable repetition rate f_t of pulse trains in a sequence. When acting on TRPA1-expressing neurons, such train sequences with $\tau_t \approx 8$ ms and $f_t \approx 1.8$ Hz were found to induce sequences of well-resolved

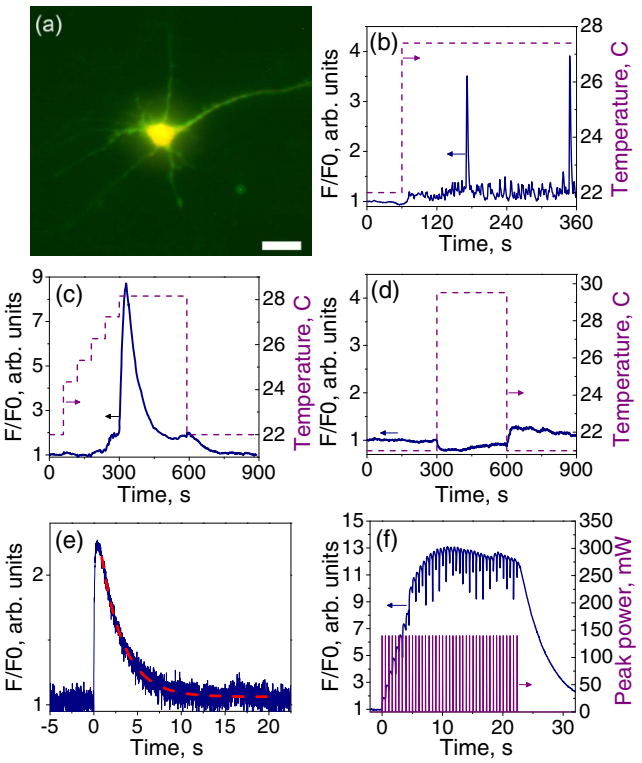

Fig. 3. (a) A GCaMP6s fluorescence image of a laser-activated neuron overlaid with a tdTomato fluorescence image of the same neuron (see Visualization 1). The scale bar is 20 μm. (b)–(d) Fluorescence of the Ca^{2+} sensor in a laser-activated neuron as a function of time (solid line) with the temperature within the laser-irradiated area inside the neuronal culture increased in a stepwise fashion (dashed line) for TRPA1-expressing neurons (b), (c) and a control neuron without TRPA1 (d). (e) A typical waveform of the Ca^{2+}-sensor fluorescence signal in response to an 8-ms, 1-mJ train of 150-fs, 78-MHz, 1450-nm OPO pulses. The dashed line shows an exponential fit with a decay half-time of 2.6 s. (f) Fluorescence of the Ca^{2+} sensor in a TRPA1-expressing neuron (navy) activated by a sequence of millisecond trains (maroon) of 78-MHz, 150-fs, 1450-nm OPO pulses with $\tau_t \approx 8$ ms and $f_t \approx 1.8$ Hz.

Ca^{2+} transients occurring at the same repetition rate f_t [Fig. 3(f)]. With a typical time of thermogenetic activation of individual neurons in our experiments [Figs. 3(c) and 3(e)] estimated as $\tau_a \approx 30$ ms, this result suggests the ways toward finely tailored (on a time scale of τ_a) thermogenetic modulation of the activity of individual neurons by using carefully sculpted near-IR laser waveforms.

To summarize, we have demonstrated a fiber-optic quantum thermometry of individual thermogenetically activated neurons based on an ODMR in fiber-coupled NV centers. Laser-induced temperature variations read out from single neurons with the NV-diamond fiber sensor have been shown to strongly correlate with the fluorescence of calcium-ion sensors, serving as online indicators of the inward Ca^{2+} current across the cell membrane of TRP-expressing neurons.

Funding. Russian Foundation for Basic Research (RFBR) (16-52-00190, 14-29-07182, 14-29-07263, 16-29-11799, 16-32-60163, 16-52-50069); Welch Foundation (A-1801); Office of Naval Research (ONR) (00014-16-1-2578).

Acknowledgment. Fluorescent microdiamonds are a gift from Columbus NanoWorks.

REFERENCES

1. A. R. Cossins, *Temperature Biology of Animals* (Chapman and Hall, 1987).
2. I. S. Ramsey, M. Delling, and D. E. Clapham, Annu. Rev. Physiol. **68**, 619 (2006).
3. E. O. Gracheva, J. F. Cordero-Morales, J. A. González-Carcacía, N. T. Ingolia, C. Manno, C. I. Aranguren, J. S. Weissman, and D. Julius, Nature **476**, 88 (2011).
4. J. Vriens, B. Nilius, and T. Voets, Nat. Rev. Neurosci. **15**, 573 (2014).
5. D. D. McKemy, W. M. Neuhausser, and D. Julius, Nature **416**, 52 (2002).
6. Y. Karashima, K. Talavera, W. Everaerts, A. Janssens, K. Y. Kwan, R. Vennekens, B. Nilius, and T. Voets, Proc. Natl. Acad. Sci. USA **106**, 1273 (2009).
7. J. C. Montgomery and J. A. Macdonald, Am. J. Physiol. **259**, R191 (1990).
8. J. G. Bernstein, P. A. Garrity, and E. S. Boyden, Curr. Opin. Neurobiol. **22**, 61 (2012).
9. D. E. Bath, J. R. Stowers, D. Hörmann, A. Poehlmann, B. J. Dickson, and A. D. Straw, Nat. Methods **11**, 756 (2014).
10. R. Chen, G. Romero, M. G. Christiansen, A. Mohr, and P. Anikeeva, Science **347**, 1477 (2015).
11. I. V. Fedotov, N. A. Safronov, Y. G. Ermakova, M. E. Matlashov, D. A. Sidorov-Biryukov, A. B. Fedotov, V. V. Belousov, and A. M. Zheltikov, Sci. Rep. **5**, 15737 (2015).
12. N. A. Safronov, I. V. Fedotov, Y. G. Ermakova, M. E. Matlashov, D. A. Sidorov-Biryukov, A. B. Fedotov, V. V. Belousov, and A. M. Zheltikov, Appl. Phys. Lett. **106**, 163702 (2015).
13. S. Chen, C. N. Chiu, K. L. McArthur, J. R. Fetcho, and D. A. Prober, Nat. Methods **13**, 147 (2016).
14. Y. Takei, S. Arai, A. Murata, M. Takabayashi, K. Oyama, S. Ishiwata, S. Takeoka, and M. Suzuki, ACS Nano **8**, 198 (2013).
15. S. Kiyonaka, T. Kajimoto, R. Sakaguchi, D. Shinmi, M. Omatsu-Kanbe, H. Matsuura, H. Imamura, T. Yoshizaki, I. Hamachi, T. Morii, and Y. Mori, Nat. Methods **10**, 1232 (2013).
16. L. Shang, F. Stockmar, N. Azadfar, and G. U. Nienhaus, Angewandte Chem. Int. Ed. **52**, 11154 (2013).
17. J.-M. Yang, H. Yang, and L. Lin, ACS Nano **5**, 5067 (2011).
18. G. Kucsko, P. C. Maurer, N. Y. Yao, M. Kubo, H. J. Noh, P. K. Lo, H. Park, and M. D. Lukin, Nature **500**, 54 (2013).
19. L. Yang, H.-S. Peng, H. Ding, F.-T. You, L.-L. Hou, and F. Teng, Microchimica Acta **181**, 743 (2014).
20. K. Okabe, N. Inada, C. Gota, Y. Harada, T. Funatsu, and S. Uchiyama, Nat. Commun. **3**, 705 (2012).
21. G. Balasubramanian, I. Y. Chan, R. Kolesov, M. Al-Hmoud, J. Tisler, C. Shin, C. Kim, A. Wojcik, P. R. Hemmer, A. Krueger, and T. Hanke, Nature **455**, 648 (2008).
22. I. V. Fedotov, S. Blakley, E. E. Serebryannikov, N. A. Safronov, V. L. Velichansky, M. O. Scully, and A. M. Zheltikov, Appl. Phys. Lett. **105**, 261109 (2014).
23. V. M. Acosta, E. Bauch, M. P. Ledbetter, A. Waxman, L.-S. Bouchard, and D. Budker, Phys. Rev. Lett. **104**, 7080 (2010).
24. E. O. Gracheva, N. T. Ingolia, Y. M. Kelly, J. F. Cordero-Morales, G. Hollopeter, A. T. Chesler, E. E. Sánchez, J. C. Perez, J. S. Weissman, and D. Julius, Nature **464**, 1006 (2010).
25. Y. G. Ermakova, D. S. Bilan, M. E. Matlashov, N. M. Mishina, K. N. Markvicheva, O. M. Subach, F. V. Subach, I. Bogeski, M. Hoth, G. Enikolopov, and V. V. Belousov, Nat. Commun. **5**, 5222 (2014).